Polystyrene-*block*-polyisoprene Nanofiber Fractions. 2. Viscometric Study

Guojun Liu* and Xiaohu Yan

Department of Chemistry, University of Calgary, 2500 University Dr., NW, Calgary, Alberta, T2N 1N4, Canada

Scott Duncan

Defense Research Development Canada−Suffield, PO Box 4000 Station Main, Medicine Hat, Alberta, T1A 8K6, Canada

Received July 26, 2002; Revised Manuscript Received January 9, 2003

ABSTRACT: The intrinsic viscosity of five well-characterized polystyrene-*block*-polyisoprene nanofiber fractions in THF was determined using viscometers of different shear rates. The values increased pronouncedly with decreasing shear rates, suggesting the ready alignment of the nanofibers along the shearing direction. The intrinsic viscosity data of the longer fractions were treated by the Yamakawa−Fujii−Yoshizaki (YFY) theory for wormlike chains to yield reasonable persistence length and hydrodynamic diameter. The validity of the YFY theory should allow the use of intrinsic viscosity in the future for evaluating the molar mass of block copolymer nanofibers.

I. Introduction

In the previous paper in this series,[1] we described the preparation of nanofibers from polystyrene-*block*-polyisoprene or PS-*b*-PI:

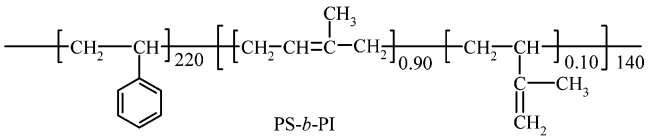

PS-*b*-PI

where PI formed cylindrical domains dispersed in the PS matrix. Nanofibers were obtained by stirring the S_2Cl_2 cross-linked PS-*b*-PI films in tetrahydrofuran (THF) to separate the cross-linked PI cylindrical domains. We also described the preparation of PS-*b*-PI nanofiber fractions with different lengths by the combined use of ultracentrifugation and ultrasonication. Transmission electron microscopy (TEM) and static light scattering (SLS) were used to obtain the length distribution $N(L_i)$, the weight-average molar mass M_w, and the *z*-average radius of gyration R_G for each fraction. Combining the $N(L_i)$ and R_G data, we also evaluated the persistence length l_P for each fraction. The nanofibers on the length scale of micrometers were shown to be semirigid or wormlike. In this paper, we report on the viscosity properties of the nanofiber fractions in THF.

Aside from a preliminary report from our group on the intrinsic viscosity of polystyrene-*block*-poly(2-cinnamoyloxyethyl methacrylate)-*block*-poly(*tert*-butyl acrylate) nanofiber fractions,[2] we are unaware of other similar studies. Won et al.[3] reported on the shear rate dependence of the viscosity of polybutadiene-*block*-poly(ethylene oxide) nanofibers in water but did not report any intrinsic viscosity data. Further, the fibers they used were not fractionated. Other more remotely related systems would be the cylindrical or wormlike micelles of block copolymers[4−8] or low molar mass surfactants.[9] The interpretation of the viscosity data of such systems has been a long-standing issue[10] mainly because of their structural instability. Alternatively, the nanofibers may be viewed as the macroscopic counterparts of polymer chains or suprapolymer chains. There are numerous examples in the literature of viscosity studies on wormlike polymer chains such as poly(*n*-hexyl isocyanate)[11,12] and Schizophyllan[13] etc. The data presented in these studies have been well interpreted by the Yamakawa−Fijii−Yoshizaki (YFY)[14,15] theory as reviewed by Bohdanecky[16]

II. Experimental Section

Materials. The solvent THF was distilled over potassium before use. The PS-*b*-PI nanofiber fractions were prepared and characterized as described before.[1] Figure 1 shows a TEM image of fraction 1 or F1. Measuring lengths of over 500 nanofibers from such TEM images at higher magnifications yielded the population density $N(L_i)$ at length L_i for each fraction. The results for F3−F5 are shown in Figure 2. The $N(L_i)$ data were then used to calculate the number-average and weight-average lengths with results shown in Table 1. Table 1 also shows the weight-average molar masses M_w and radii of gyration R_G determined by static light scattering for the nanofibers in THF.

The radii of gyration R_G were previously related to the persistence lengths l_P wrongfully using[1]

$$R_G(l_P) = \frac{\sum_i N(L_i) L_i^2 R_G(L_i, l_P)}{\sum_i N(L_i) L_i^2} \quad (1)$$

The correct relation is

$$R_G(l_P) = \left(\frac{\sum_i N(L_i) L_i^2 R_G^2(L_i, l_P)}{\sum_i N(L_i) L_i^2} \right)^{1/2} \quad (2)$$

where $R_G(l_P)$ equals R_G determined from light scattering.

10.1021/ma021202d CCC: $25.00
Published on Web 02/15/2003

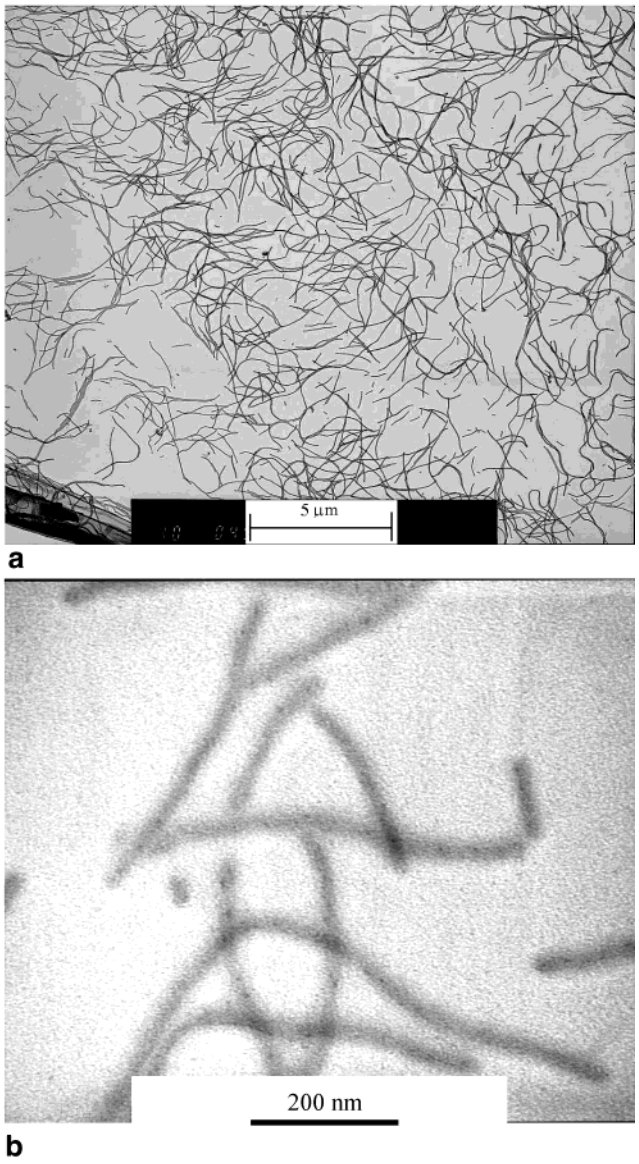

Figure 1. TEM images of PS-*b*-PI nanofiber fraction 1 at different magnifications. The sample was aspirated from THF and stained with OsO_4.

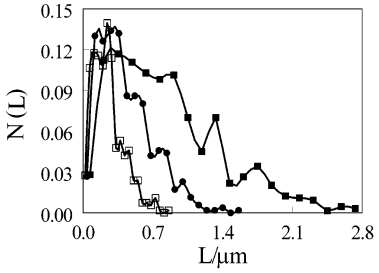

Figure 2. Length distribution functions for nanofiber fractions 3 (■), 4 (●), and 5 (□), respectively.

$R_G(L_i,l_P)$ in eq 2 was approximated by[17]

$$R_G(L,l_P) = l_P\sqrt{L/3l_P - 1 + (2l_P/L)[1 - (l_P/L)(1 - e^{-(L/l_P)})]} \quad (3)$$

which is valid for infinitely thin chains. Figure 3 plots the $R_G(l_P)$ function given by eq 2. Checking the experimental R_G values against l_P in Figure 3 yielded for the fractions the l_P values shown in Table 1.

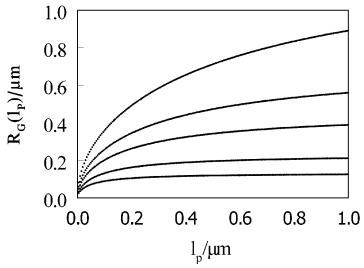

Figure 3. From top to bottom, plot of R_G calculated from eq 2 as a function of persistence length l_P for fractions 1−5, respectively.

Table 1. Characteristics of the PS-*b*-PI Nanofiber Fractions

sample	TEM L_W (nm)	TEM L_N (nm)	M_w (g/mol)	R_G (nm)	l_p (nm)
F1	3110	1970	8.5×10^8	427	145
F2	1760	1210	4.9×10^8	347	205
F3	1190	840	3.7×10^8	280	242
F4	600	430	2.2×10^8	171	245
F5	340	250	1.2×10^8	117	390

Table 2. Characteristics of the Ubbelohde Capillary viscometers

property	viscometer 1	viscometer 2	viscometer 3
capillary length (cm)	8.4	35.9	112.3
bulb vol (mL)	1.50	1.21	0.71
THF flow time (s)	267.50	241.47	336.46
THF flow rate Q (mL/s)	5.61×10^{-3}	5.01×10^{-3}	2.11×10^{-3}
capillary radius R (mm)	0.155	0.185	0.185
shear rate (s^{-1})	1920	1010	420

We have also performed the linear regression analysis of the M_w vs L_w data,[1] which yielded the unit-length molar mass of 2.7×10^{12} g/(mol·cm) for the nanofibers. Analysis of a transmission electron microscopy (TEM) image of a PS-*b*-PI thin section yielded the diameter of 12.1 nm for the PI cylinders dispersed in the PS matrix.

Ubbelohde Capillary Viscometers. Three Ubbelohde capillary viscometers were used in this study. Table 2 summarizes the characteristics of the viscometers. To determine the bulb volume, a concentrated polystyrene (PS) solution, e.g., at ∼20 wt %, in THF was added into the viscometer reservoir. The solution was pressured into the capillary and methanol was dispensed from the top of the capillary, which induced PS chain aggregation at the THF/methanol interface and capillary blockage. The bulb was then filled with methanol for volume determination. The volume was used to calculate the flow rate Q from diving it by the THF flow time. The shear rate at the capillary wall was calculated using[18]

$$\tau = \frac{4Q}{\pi R^3} \quad (4)$$

where R is the capillary radius. The shear rates of the three viscometers are 1920, 1010, and 420 s^{-1}, respectively, for THF flow at 25.0 ± 0.1 °C.

Rotational Cylinder Viscometer. A low-shear-rate rotational cylinder viscometer was built based on a design by Zimm and Crothers.[19] The stationary part or the stator of the viscometer consists of a jacketed one-end-sealed glass cylinder with an inner diameter, d_o, of 1.24 cm. Water was allowed to circulate in the jacketed layer for temperature control. The moving part or the rotor of the viscometer is a 8.4 cm-long one-end-sealed cylinder with an outer diameter, d_{in}, of 1.00 cm. Glued to bottom of the rotor is a steel pellet. The inner cylinder floats in the stator by its buoyancy and its height is adjusted by the amount of Pb_3O_4 fixed in it by epoxy resin. The rotor is held in the center of the stator by the surface forces exerted by the testing liquid. The inner cylinder rotates

Table 3. Viscosity Results of the Nanofiber Fractions in THF, where the Intrinsic Viscosity Data Are in mL/g

	shear rate = 1920 s^{-1}		shear rate = 1130 s^{-1}		shear rate = 420 s^{-1}		shear rate = 0.47 s^{-1}		shear rate = 0.16 s^{-1}		shear rate = 0.082 s^{-1}		l_P
sample	$[\eta]$	k_h	$[\eta]$	k_h	$[\eta]$	k_h	$[\eta]$	k_h	$[\eta]$	k_h	$[\eta]_0$	k_h	(nm)
F1	101	0.58	127	0.37			379	1.26	627	0.42	648	0.45	720
F2	56.5	0.65	64.5	0.57	77.5	0.47	192	0.81			321	0.41	570
F3	42.9	0.36	52.7	0.56	65.2	0.26	138	1.44			246	0.54	900
F4	27.5	0.80	35.2	0.44	42.1	0.64	83	1.71			140	0.47	*a*
F5	17.3	3.3	24.2	2.57	29.3	1.21	56	1.87			98	0.78	*a*

[a] The highest $[\eta]$ that can be reached from eq 16 by assuming rigid-rod behavior and $d_h = 97$ nm for the two fractions are ~136 and ~75 mL/g, respectively.

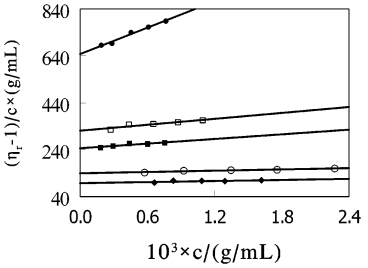

Figure 4. Plot of $(\eta_r - 1)/c$ vs c for the nanofiber solutions in THF. The data were obtained using the cylindrical viscometer at a shear rate of 0.082 s^{-1}. From top to bottom are the data for F1 (●), F2 (□), F3 (■), F4 (○), and F5 (◆), respectively.

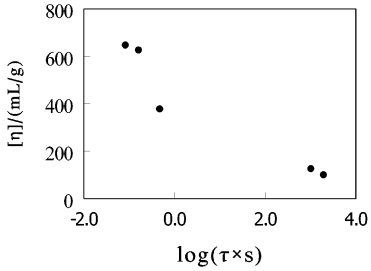

Figure 5. Plot of $[\eta]$ vs $\log(\tau \times s)$ for nanofiber fraction 1 in THF.

relative to the stator because of a rotating magnetic field applied at the bottom of the viscometer. Since there are no mechanical devices attached to the rotor, frictional dissipation of energy occurs in the liquid itself, and the viscosity of a liquid is proportional to the time it takes for the rotor to make one circle relative to the stator. The rotor speed was adjusted by changing the size of the steel pellet in the rotor.

The shear rate of the viscometer at the inner wall of the stator was estimated using[18]

$$\tau = \frac{4\pi/t_c}{(d_o/d_{in})^2 - 1} \tag{5}$$

where t_c denotes the time taken for the rotor to rotate one cycle. Three rotors with the t_c values of 51.29, 148.42, and 283.41 s and thus the shear rates of 0.47, 0.16, and 0.082 s^{-1} were obtained.

Viscosity Measurements. All viscosity measurements were performed at 25.0 ± 0.1 °C in THF. The nanofiber concentrations were so adjusted that the relative viscosity η_r of the most concentrated solution was around ~1.4.

III. Results and Discussion

Results. Figure 4 plots $(\eta_r - 1)/c$ against nanofiber concentration c, where η_r was determined in THF using the cylindrical viscometer at the shear rate of 0.082 s^{-1}. Like polymer solutions, the data for each fraction fall on a straight line. The solid lines represent the best fit to the experimental data by the empirical relation[20]

$$(\eta_r - 1)/c = [\eta] + k_h[\eta]^2 c \tag{6}$$

where k_h is the Huggins coefficient and $[\eta]$ is the intrinsic viscosity. Similar plots were obtained for data obtained from the other viscometers. Table 3 summarizes the $[\eta]$ and k_h results for all samples thus obtained at different shear rates.

Table 3 reveals that the $[\eta]$ values of the nanofibers are strongly shear-rate τ dependent, i.e., $[\eta]$ increased with decreasing τ. Figure 5 plots $[\eta]$ for F1 as a function of τ. The $[\eta]$ values appear to level off only at the lowest τ of 0.082 s^{-1} and the $[\eta]$ values at this τ are used to approximate the zero-shear intrinsic viscosity $[\eta]_0$. We had not measured $[\eta]$ at lower τ values, as the balance of rotors with slower rotation rates presented much technical challenge. Furthermore, we expected our samples to behave similarly as bacteriophase T2 DNA in water. For the DNA, $[\eta]$ values were found to be at 97% and 99% of the $[\eta]_0$ values at the shear rates of 0.165 and 0.08 s^{-1}, respectively.[19,21]

While the k_h values measured at 0.47 s^{-1} are larger than 0.55, the k_h values determined at the two lowest shear rates, except that for F5, are normal between 0.30 and 0.55.[22] The abnormally high k_h at 0.47 s^{-1} suggests a strong shear rate dependence of viscosity in the neighborhood of this τ. In this case, the rotor rotates faster in a more dilute solution not only for the lower solution concentration but also for the higher shear rate the solution experiences. The negative deviation of the apparent relative viscosity η_r from the zero-shear-rate $\eta_r(\tau \to 0)$ gets larger and larger as the concentration is decreased. This systematic error in η_r leads to a steeper $(\eta_r - 1)/c$-vs-c line, which results in a larger slope and smaller intercept $[\eta]$. The normal k_h values at the two lowest τ values suggest weak τ dependence of nanofiber solution viscosity in the neighborhood of these τ values.

The k_h value of F5 is abnormal irrespective of τ. This may be due to the small length to diameter or aspect ratio for this fraction. Thus, this sample may not have viscosity properties similar to those of polymers.

The pronounced decrease in $[\eta]$ of a sample with decreasing τ at τ larger than ~0.16 s^{-1} suggests the ready alignment of the nanofibers along the shearing direction as has been demonstrated for PS-*b*-PCEMA nanofibers,[23] or cylindrical domains in diblock copolymer matrices.[24] The η_r value increased with decreasing shear rate, because nanofibers are more randomized in orientation at lower shear rates and the randomized fibers impose greater flow resistance.

YFY Theory. The theoretical expressions for the zero-shear intrinsic viscosity $[\eta]_0$ were first derived by Yamakawa and Fujii[14] for wormlike polymer chains and later refined by Yamakawa and Yoshizaki[15] to accommodate spheroid cylinders, which are cylinders with spheroidal end caps. For spheroid cylinders

$$[\eta]_0 = \frac{\pi N_A L^2}{24 M_U} f(L/l_P) F(L/d_h,\epsilon) \quad \text{if } L/l_P \le 4.556 \quad (7)$$

and

$$[\eta]_0 = \frac{8\phi_0 l_P^{3/2} L^{1/2}}{M_U}\left(1 - \sum_{j=1}^{4} C_j (L/l_P)^{-j/2}\right)^{-1} \quad \text{if } L/l_P \ge 4.556 \quad (8)$$

where N_A is Avogadro's constant, d_h is the hydrodynamic diameter of the cylinder part, $\phi_0 = 2.870 \times 10^{23}$ mol^{-1}, C_j is a polynomial function of d_h/l_P, and ϵ is the ratio of the principal diameters of the spheroidal ends. The expressions for $f(L/l_P)$, $F(L/d_h,\epsilon)$, and C_j have been given in ref 15 and are thus not repeated here. The YFY theory has been used to treat the intrinsic viscosity data of various wormlike polymer chains to yield reasonable l_P and d_h values.[16] The theory has, however, never been used to treat cross-linked cylindrical micelles or nanofibers.

Data Treatment by the Bohdanecky Method. Equations 7 and 8 for $[\eta]_0$ derived by YFY are complex. Bohdanecky[16] determined that the YFY expressions could be cast in a much simpler form:

$$(M_w^2/[\eta]_0)^{1/3} = A + B M_w^{1/2} \quad (9)$$

where

$$A = A_0 M_U/\phi_0^{1/3} \quad (10)$$

and

$$B = B_0\sqrt{M_U}/(\phi_0^{1/3}\sqrt{2 l_P}) \quad (11)$$

In eqs 10 and 11

$$A_0 = 0.46 - 0.53 \log d_r \quad (12)$$

and

$$B_0 = 1.00 - 0.0367 \log d_r \quad (13)$$

where d_r, equal to $d_h/(2l_P)$, is the reduced hydrodynamic diameter of the chains.

Figure 6 plots the intrinsic viscosity data of the nanofiber fractions following eq 9. Excluding the data for F5, which has abnormal viscosity behavior, the other data points all fall on a straight line. The A and B values generated depended on the data points used in the linear regression analysis (Table 4). Using the A and B values and eqs 10−13, we obtained the l_P and d_h values of 620 and 97 nm, if only the F1−F3 data were used. The l_P and d_h values changed to 606 and 178 nm when the F1−F4 data were used. The small difference between the two l_P values suggests that $l_P$can be determined with certainty from the data. The d_h value is determined with much reduced certainty, because it changes exponentially with the intercept A.

Estimation of d_h. Figure 1b shows a TEM image of the F1 nanofibers sprayed from THF at high magnification. The diameter of the visible part of the nanofibers is 25.2 ± 1.4 nm. Since the sample was stained with OsO_4, which reacted with the unreacted PI double bonds, and also the S and Cl atoms incorporated via the cross-linking reactions are heavier than the C and H atoms in the PS block, the visible part of the fibers must be cross-linked PI. As mentioned in ref 1, the diameter of the PI cylindrical domains in the diblock film is 12.1 nm. After cross-linking with S_2Cl_2, the PI diameter should increase somewhat. The core diameter should increase further in THF. The TEM specimens were prepared by the quick aspiration of the nanofibers from THF on to carbon-coated copper grids,[25] which might have left the core trapped in a partially or fully swollen state. Thus, the TEM core diameter of ∼25 nm is reasonable.

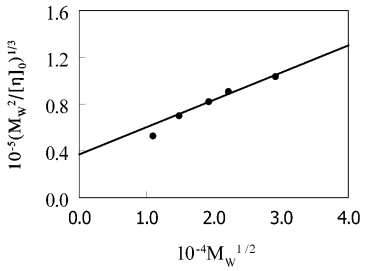

Figure 6. Plot of $(M_w^2/[\eta]_0)^{1/3}/(g/(mol^{2/3}\cdot cm))$ vs $M_w^{1/2}/(g/mol)^{1/2}$ for the nanofiber fractions. The solid line represents the best fit to the F1−F4 data by eq 9.

Table 4. Parameters Generated from the Analysis of the $[\eta]_0$ Data Using Eq 9

data range	A (g/mol$^{2/3}$·cm)	B (g$^{1/2}$/mol$^{1/6}$·cm)	fitting coeff χ^2	l_P (nm)	d_h (nm)
F1−F3	4.29×10^4	2.10	0.993	620	97
F1−F4	3.69×10^4	2.33	0.993	606	178

The molar mass of the PS-*b*-PI diblock is 3.24×10^4 g/mol. The M_U value of the nanofiber is 2.7×10^{12} g/(mol·cm). Using these values and assuming a core diameter of 25 nm for the nanofibers in THF, we calculated a PS coverage ρ of 2.12×10^{13} chains/cm^2 on the core surface. The critical surface coverage ρ^* above which PS chains begin to overlap and repel one another is[26]

$$\rho^* = \frac{1}{\pi R_G^2} \quad (14)$$

where R_G is the radius of gyration of an unperturbed PS chain. For PS in good solvent

$$R_G = N_{PS}^{0.60}\beta \quad (15)$$

where N_{PS}, equal to 220 here, is the number of styrene units in a chain, and β, the segment length, is 0.186 nm as reported by Higo et al.[27] in toluene. Combining eqs 14 and 15, we obtained $\rho^* \approx 1.4 \times 10^{12}$ chains/cm^2. Since ρ is much larger than ρ^*, the PS chains should form a brush layer on the core surfaces.

The chains in a brush layer are stretched. The degree of stretching depends on the surface coverage. Taunton et al.[28] found, from surface force measurement, that the average end-to-end distance for an end-anchored PS sample at $M_w = 2.65 \times 10^4$ g/mol was 22 nm. The surface coverage might be higher[29] in our case, but the PS molar mass is slightly lower; i.e., at 2.3×10^4 g/mol, the PS coronal layer thickness of ∼22 nm should thus be a reasonable estimate. While 22 nm is substantially larger than ∼10 nm estimated for unperturbed chains, it is still substantially less than the fully stretched chain length of ∼55 nm.

On the basis of the PS layer thickness of ~22 nm and the core diameter of ~25 nm, we estimated that the hydrodynamic diameter of a PS-*b*-PI nanofiber in THF should be ~70 nm. This value agrees reasonably well with $d_h = 97$ nm determined from the F1−F3 viscosity data, given the error involved with d_h determination and estimation. The analysis, however, rules out the possibility for having $d_h = 178$ nm. Thus, F4 may still have too low an aspect ratio to qualify for data treatment by the Bohdanecky method by assuming polymer chain behavior.

Data Treatment by the YFY Theory. The key equations of the YFY theory have been given above already. For convenience, we assumed in our calculations that the ends of the PS-*b*-PI nanofibers were hemispherical or $\epsilon = 1$, despite the fact that this was most likely untrue for ultrasonicated samples. To account for length distribution of each fraction, the experimental intrinsic viscosity was calculated using:

$$[\eta]_0 = \frac{\sum_i [\eta]_{i0} N(L_i) L_i}{\sum_i N(L_i) L_i} \qquad (16)$$

where $[\eta]_0$ is the weight-average[20a] of the components $[\eta]_{i0}$ and $N(L_i)$ is proportional to the population of fibers with contour length L_i.

Using $d_h = 97$ nm, $M_U = 2.7 \times 10^{12}$ g/(mol·cm), $N(L_i)$, and eq 16, we evaluated the persistence lengths for F1−F3 with results shown in Table 3. The average of the l_P values for the three fractions is ~700 nm and the value fluctuates much from sample to sample.

Unfortunately, the highest $[\eta]_0$ values that can be reached from eq 16 by assuming $d_h = 97$ nm, $M_U = 2.7 \times 10^{12}$ g/(mol·cm) and rigid rod behavior for F4 and F5 are 136 and 75 mL/g, respectively, which are lower than the experimental values. The discrepancy may be due to the low aspect ratio L_n/d_h and $\epsilon \neq 1$ for these samples.

Difference between the l_P Values from SLS and Viscometry. The l_P value from treating the viscosity data using the Bohdanecky method is ~620 nm. This compares well with ~400 nm we estimated before for polystyrene-*block*-poly(2-cinnamoyloxyethyl methacrylate) nanofibers[23] and ~570 nm determined by Won et al.[3] for poly(ethylene oxide)-*block*-polyisoprene nanofibers. The value is, however, significantly larger than the value of ~250 nm that we determined from LS. The LS values may be less accurate for the following reasons. First, we are less confident about the R_G values of F1−F3, because the sizes of these fractions might be beyond the resolution range of our instrument with the lowest accessible scattering angle at 12°. The R_G values of F4 and F5 can be determined with higher accuracy but they do not fall in the region of the R_G-vs-l_P curve where R_G changes sensitively with l_P (Figure 3). While $l_P = 390$ nm at $R_G = 117$ nm for F5, the l_P value, for example, increases to 620 nm if $R_G = 122$ nm.

Scaling Relation for $[\eta]_0$. The accurate equation relating $[\eta]_0$ and L and thus M_w is given by eqs 7 and 8. A scaling relation between $[\eta]_0$ and M_w is eq 9. It reduces to the scaling relation $[\eta]_0 \propto M_w^{1/2}$ as $M_w \rightarrow \infty$. Over a particular range with intermediate M_w, the Kuhn−Mark−Houwink−Sadara scaling relation may hold:[20]

$$[\eta]_0 = K M_w^{\ a} \qquad (17)$$

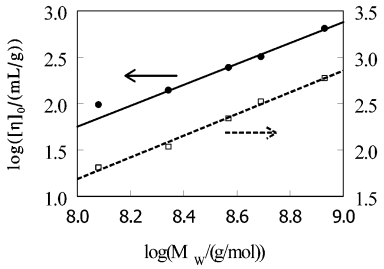

Figure 7. Plot of $\log[\eta]_0$ vs $\log M_w$ for the nanofiber fractions. The theoretical $[\eta]_0$ values (□) were calculated from eqs 7, 8, and 16 letting $l_P = 620$ nm and $d_h = 97$ nm. Only the F1−F4 experimental $[\eta]_0$ data (●) were used in the curve fitting.

The exponent a in eq 17 provides a measure of the flexibility of the fibers in the particular length range. If the a scale of polymer chains can be borrowed at all, an a value in the range of 0.50 to 0.764 suggests chain flexibility.[20] Wormlike fibers would have a values greater than 0.764. It approaches the limiting value of 2.0 for rigid rods.

Illustrated in Figure 7 is a plot of $\log [\eta]_0$ vs $\log M_w$ for the nanofiber fractions. A straight line fit to the data of F1−F4 yielded an a value of 1.13, suggesting the wormlike nature of the fibers. The F5 data was excluded in curve fitting as the $[\eta]_0$ value is in error due to the low aspect ratio L_n/d_h for this fraction. Also shown for comparison are the $\log [\eta]_0$ data with $[\eta]_0$ calculated using eq 16 by assuming $l_P = 620$ nm and $d_h = 97$ nm. The a value obtained from fitting the calculated data is 1.17, which again confirms the wormlike nature of the nanofibers in the molar mass range of 1.2×10^8 to 8.5×10^8 g/mol.

IV. Conclusions

The intrinsic viscosity $[\eta]$ of five PS-*b*-PI nanofiber fractions in THF was determined with viscometers of different shear rates τ and $[\eta]$ increased drastically with decreasing τ. This suggests the ready alignment of the nanofibers along the shearing direction. The $[\eta]$ values at the lowest shear rate of 0.082 s^{-1} were used to approximate the zero-shear intrinsic viscosity $[\eta]_0$. The $[\eta]_0$ data were treated with both the Bohdanecky method and the YFY theory to yield a reasonable persistence length value ~620 nm. The hydrodynamic diameter d_h of 97 nm determined using the F1−F3 data from the Bohdanecky method was reasonable but the uncertainty involved was large. While the YFY theory may be applicable to block copolymer nanofiber solutions and the potential exists for the use of intrinsic viscosity in the future to determine the molar mass of nanofibers, more studies are required to confirm the true applicability of the YFY theory.

Acknowledgment. The NSERC of Canada and Defense Research Development Canada are cordially acknowledged for sponsoring this research

References and Notes

(1) Liu, G. J.; Yan, X. H.; Duncan, S. *Macromolecules* **2002**, *35*, 9788.
(2) Liu, G. J.; Yan, X. H.; Qiu, X. P.; Li, Z. *Macromolecules* **2002**, *35*, 7742.
(3) Won, Y.-Y.; Davis, H. T.; Bates, F. S. *Science* **1999**, *283*, 960.
(4) Price, P. *Pure Appl. Chem.* **1983**, *55*, 1563.
(5) Zhang, L. F.; Eisenberg, A. *Science* **1995**, *268*, 1728.
(6) Massey, J.; Power, K. N.; Manners, I.; Winnik, M. A. *J. Am. Chem. Soc.* **1998**, *120*, 9533.

(7) Ding, J. F.; Liu, G. J.; Yang, M. L. *Polymer* **1997**, *38*, 5497.
(8) (a) Tao, J.; Stewart, S.; Liu, G. J.; Yang, M. L. *Macromolecules* **1997**, *30*, 2738. (b) Stewart, S.; Liu, G. J. *Angew. Chem., Int. Ed.* **2000**, *39*, 340. (c) Liu, F. T.; Liu, G. J. *Macromolecules* **2001**, *34*, 1302.
(9) For review articles on this subject, see, for example: (a) Gelbart, W. M.; Ben-Shaul, A. *J. Phys. Chem.* **1996**, *100*, 13169. (b) Israelachvili, J. N.; Mitchell, D. J.; Ninham, B. W. *J. Chem. Soc., Faraday Trans. 1* **1976**, *72*, 1525.
(10) See, for example: Duyndam, A.; Odijk, T. *Langmuir* **1996**, *12*, 4718.
(11) Kuwata, M.; Murakami, H.; Norisuye, T.; Fujita, H. *Macromolecules* **1984**, *17*, 2731.
(12) Ohshima, A.; Kudo, H.; Sato, T.; Teramoto, A. *Macromolecules* **1995**, *28*, 6095.
(13) Yanaki, T.; Norisuye, T.; Fujita, H. *Macromolecules* **1980**, *13*, 1462.
(14) Yamakawa, H.; Fujii, M. *Macromolecules* **1974**, *7*, 128.
(15) Yamakawa, H.; Yoshizaki, T. *Macromolecules* **1980**, *13*, 633.
(16) Bohdanecky, M. *Macromolecules* **1983**, *16*, 1483. The application of the Yamakawa−Fujii−Yoshizaki theory to many wormlike chain systems is discussed.
(17) Benoit, H.; Doty, P. *J. Phys. Chem.* **1953**, *57*, 958.
(18) See, for example: Rodriguez, F. *Principles of Polymer Systems*, 4th ed.; Taylor & Francis, Washington, DC, 1996.
(19) Zimm, B. H.; Crothers, D. M. *Proc. Nat. Acad. Sci.* **1962**, *48*, 905.
(20) See, for example: (a) Elias, H. G. *An Introduction to Polymer Science*; VCH: Weinheim, Germany, 1997. (b) Sperling, L. H. *Introduction to Physical Polymer Science* John Wiley & Sons: New York, 1992.
(21) Crothers, D. M.; Zimm, B. H. *J. Mol. Biol.* **1965**, *12*, 525.
(22) Moore, W. R. In *Progress in Polymer Science*; Jenkins, A. D.; Ed. Pergamon Press: Oxford, England, 1969; Vol. 1, p 1.
(23) Liu, G. J.; Ding, J.; Qiao, L.; Guo, A.; Gleeson, J. T.; Dymov, B.; Hashimoto, T.; Saijo, K. *Chem.−Eur. J.* **1999**, *5*, 2740.
(24) See, for example: (a) Winter, H. H.; Scott, D. B.; Gronski, W.; Okamoto, S.; Hashimoto, T. *Macromolecules* **1993**, *26*, 7236. (b) Morkved, T. L.; Lu, M.; Urbas, A. M.; Ehrichs, E. E.; Jaeger, H. M.; Mansky, P.; Russell, T. P. *Science* **1996**, *273*, 931.
(25) Ding, J. F.; Liu, G. J. *Macromolecules* **1999**, *32*, 8413.
(26) (a) De Gennes, P. G. *Macromolecules* **1980**, *13*, 1069. (b) Milner, S. T. *Science* **1991**, *251*, 905.
(27) (a) Higo, Y.; Ueno, N.; Noda, I. *Polym. J.* **1983**, *15*, 367. (b) Parsonage, E.; Tirrell, M.; Watnabe, H.; Nuzzo, R. G. *Macromolecules* **1991**, *24*, 1987.
(28) Taunton, H. J.; Toprakcioglu, C.; Fetters, L. J.; Klein, J. *Macromolecules* **1990**, *23*, 571.
(29) To see some typical experimental ρ/ρ^* values for self-assembled brushes, refer to, for example: (a) Tao, J.; Guo, A.; Stewart, S.; Birss, V. I.; Liu, G. J. *Macromolecules* **1998**, *31*, 172. (b) Ding, J. F.; Birss, V. I.; Liu, G. J. *Macromolecules* **1997**, *30*, 1442. (c) Ding, J. F.; Tao, J.; Guo, A.; Stewart, S.; Hu, N.; Birss, V. I.; Liu, G. J. *Macromolecules* **1996**, *29*, 5398. (d) Tao, J.; Guo, A.; Liu, G. J. *Macromolecules* **1996**, *29*, 1618.

MA021202D